Journal of Low Temperature Physics
https://doi.org/10.1007/s10909-020-02337-1

Thermal Impact of Cosmic Ray Interaction with an X-Ray Microcalorimeter Array

Antoine R. Miniussi[1,2] · Joseph S. Adams[1,2] · Simon R. Bandler[1] · Sophie Beaumont[1,2] · Meng P. Chang[1,3] · James A. Chervenak[1] · Fred M. Finkbeiner[1,4] · Jong Y. Ha[1,5] · Ruslan Hummatov[1,2] · Richard L. Kelley[1] · Caroline A. Kilbourne[1] · Frederick S. Porter[1] · John E. Sadleir[1] · Kazuhiro Sakai[1,2] · Stephen J. Smith[1,2] · Nicholas A. Wakeham[1,2] · Edward J. Wassell[1,3]

Received: 18 July 2019 / Accepted: 13 January 2020

Abstract

The X-ray Integral Field Unit (X-IFU) instrument on the Athena mission will be positioned at the Lagrangian point L2 and be subject to cosmic rays generated by astrophysics sources, primarily relativistic protons. Previous simulations have shown that particles of energy higher than 150 MeV will make it through the outer layers of the satellite. They will reach the detector wafer with a rate of 3 cts cm^{-2} s^{-1} and a most probable energy deposited in the Si frame supporting the array at 150 keV. These events can affect the energy resolution of the detectors through the thermal fluctuations that they produce. This study assesses this potential problem and discusses two suggested design approaches to decrease the impact of cosmic ray in order to limit their effect to their allocation of 0.2 eV within the Athena/X-IFU energy-resolution budget. The first is the addition of a coating layer of high heat capacity material (e.g., Pd) and the second is the splitting of this coating into two thermal regions near the TES array to keep the heat away from the array. Implementing these two features is predicted to cause a decrease in the number of events above 1 μK by more than a factor 10 to ~1.5 cps when compared to an equivalent design without these features.

Keywords Cosmic rays · TES · Athena/X-IFU · Thermal model · Cryogenics

✉ Antoine R. Miniussi
antoine.r.miniussi@nasa.gov

[1] NASA Goddard Space Flight Center, Greenbelt, USA

[2] CRESST II – University of Maryland Baltimore County, Baltimore, USA

[3] SSAI Science Systems and Applications, Inc., Hampton, USA

[4] Sigma Space Corp., Lanham, USA

[5] SB Microsystems, Ferndale, USA

Published online: 13 February 2020

1 Cosmic Ray Interaction with the Detector Wafer

In the foreseen orbits for the Athena mission [1] and its X-ray Integral Field Unit (X-IFU) instrument [2] around Lagrange points L2, the cosmic ray (CR) background consists mainly of protons. Simulations run under GEANT4 have shown that under solar minimum conditions (maximum CR flux [3]) protons above ~ 150 MeV [4] can penetrate the cryostat and reach the sensor array wafer at a rate of ~ 3 cps per cm^2. With a surface of ~ 64 cm^2, the whole wafer could be hit at a rate of 190 cps [5]. A numerical spectrum of the deposited energy in the wafer, computed over 83 s for the current characteristics of the detector array, is shown in Fig. 1. The peak of the deposited energy in the Si substrate is around 150 keV.

The wafer is a 61 cm^2 hexagon composed of a 300 µm thick silicon substrate and a 0.5 µm thick Si_3N_4 membrane. The outer part of the wafer is called the *frame*. The wafer supports at its center a 3 cm^2 hexagonal array of thousands of superconducting transition-edge sensor (TES) microcalorimeters. These detectors are each composed of a Mo/Au bilayer, as the sensing thermistor, and a Bi/Au X-ray absorber attached to it. Under each TES, the Si substrate is completely etched, up to the Si_3N_4. The resulting structures, part of the Si layer, are called muntins. Each TES is then suspended on the frame by the silicon nitride membrane which becomes the main thermal contact between the TES and the bath at 55 mK [6]. The back of the Si frame is coated with a Au layer of thickness varying from 2 to 6 µm to improve the heat dissipation inside it. Numerous gold wirebonds thermally link the Au coating to the cryostat's cold finger at 55 mK.

The CRs that pass through the TES microcalorimeters are detected by the Cryogenic Anticoincidence detector (CryoAC) [7] that is located underneath the array at

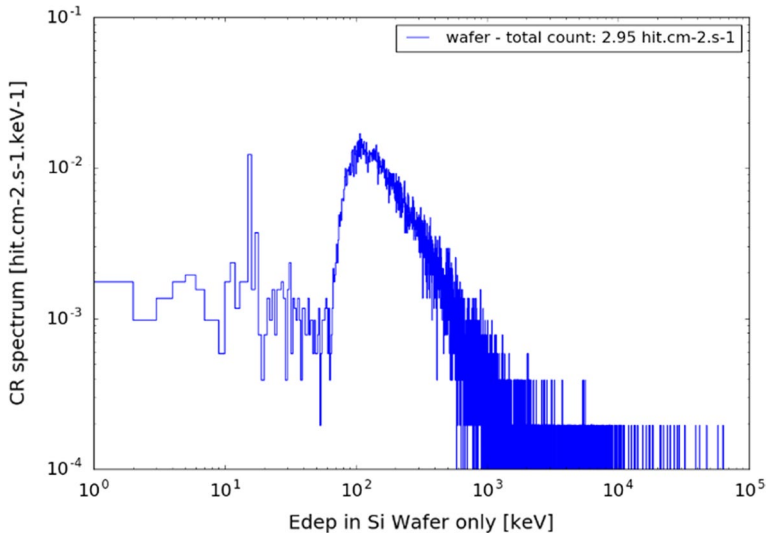

Fig. 1 Spectrum of deposited energies in the 300 µm thick Si wafer by primary and secondary hits during a solar minimum. Generated by Monte Carlo simulation under GEANT4 (Color figure online)

a distance of 1 mm over a surface of ~7 cm^2. However, the hits occurring outside of the microcalorimeter array, in the frame, will not be flagged but can still impact the thermal bath of the detectors. This study is here to assess this effect and demonstrate the ways to mitigate the thermal impact.

With an allocation of 0.2 eV within the Athena/X-IFU energy-resolution budget and a thermal sensitivity of the TES microcalorimeters of 0.15 eV/μK, the scientific data can be significantly impacted.

2 Description of the Thermal Model of the Microcalorimeter Array and Its Substrate

2.1 Details of the Model

We have developed a 2D thermal model to investigate the effects of the CRs using the finite element software Comsol Multiphysics [8]. It is composed of two hexagons representing the TES microcalorimeter array surrounded by the frame (see Fig. 2, left). The different layers of material are modeled as distinct thermal blocks connected to each other through thermal links as represented in Fig. 2, right. This model considers the Si layer of 300 μm, the Si_3N_4 membrane of 0.5 μm, the electron and phonon components of the Au coating, the number of wirebonds and the TES. The muntin width is 108 μm. Figure 3 shows a diagram of these different elements. The TES microcalorimeter is merged into one block since the absorber dominates the total heat capacity by a factor 100 and the thermal conductivity between

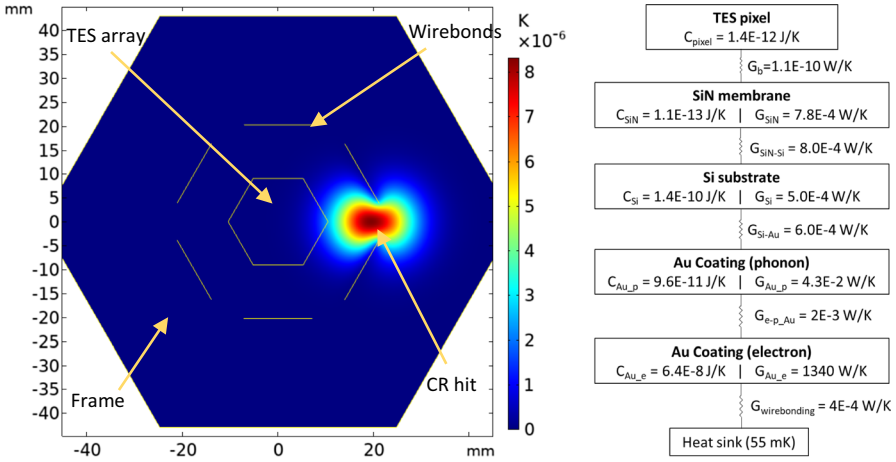

Fig. 2 Left, Thermal diffusion 25 μs after a CR hit deposition of 150 keV at 20 mm away from the center of the TES array. The color scale gives the elevation of temperature above 55 mK. The biggest hexagon represents the wafer while the smaller one represents the TES array. The muntins are represented as a 2D region on which are applied factors on the heat capacity and thermal conductivity to properly model the thermal behavior of the muntins and the coating on it. The 6 lines around the TES array are the position of potential wirebonds which heatsink the wafer. Right, thermal block diagram of the different layers of the model (Color figure online)

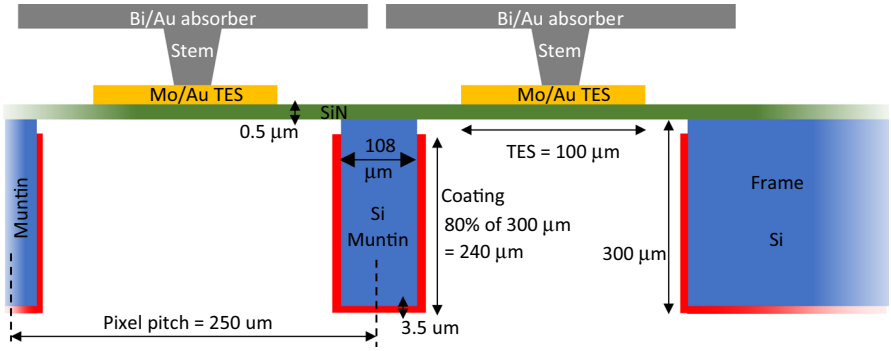

Fig. 3 Schematic of two TES on the side of the array. The right one is near the Si frame, the left one is surrounded by Si muntins. The Si_3N_4 membrane supports the bilayer Mo/Au TES. The absorber is mechanically and thermally connected to the TES by a Au stem. The Au coating covers the bottom of each muntin and their side up to 80% due to the deposition angle as well as the frame (Color figure online)

the absorber and the TES can be considered as infinite. Some of the features on the frame such as the hole, bond pads, etc. are not included because they are not large enough to significantly affect the thermal design. The main parameters studied were the thickness variation of the Au coating between 3.5 and 6 µm, the number of wire-bonds from 500 to 2000 and their location.

2.2 Validation of the Model

To validate our general approach, we used the same technique to model the Hitomi detector chip [9] for which we have experimental ground data. The detector chip was loaded with a heater and a calibration pixel to study its thermal behavior through heat pulses. A numerical model was developed to represent the Hitomi wafer and the thermal links between the different blocks. It reproduced within a factor 2.5 the amplitude of the heat pulse measured on the calibration pixel and within 10% of its time constant. Given the complexity of the model and the uncertainty on some of the parameters, this is a reassuring result, since the model appears to err on the conservative side, meaning that the modeled effects were larger than the effects actually seen from known energy depositions.

3 Impact of the CR Hit on the Detector

3.1 Description of the Analysis

In order to measure the impact of a CR event on the data, several steps are required. Using the distribution of deposited energy provided by INAF (Fig. 1), the local temperature increase due to a CR impact at a distance d and angle θ from the impact site is computed. To decrease the computing time, we choose to use a symmetrical

geometry. The hexagonal wafer is then modeled as a circle (see Fig. 6, left). As we can see in Fig. 8, right, this has no significant impact on the computed temperature changes or thermal relaxation time constants. The thermal increase in the bath for several CR hit locations and energies are examined at the center of the TES array and the edge.

The output data from the thermal model can be interpolated to compute the temperature profile of the thermal bath for any CR hit location and energy. These interpolation tables are used by the "End-to-End simulator" previously developed to model the performance of the microcalorimeter pixels. [10–12]. This simulator computes how the energy of an X-ray event, measured with optimal filtering, is affected by the thermal bath fluctuation caused by CRs, randomly distributed spatially across the frame of the hexagonal Si substrate and temporally relative to the arrival time of the X-ray. This last part of the analysis is reported in [13].

3.2 Location and Number of Wirebonds

The locations of the wirebonds shown in Fig. 6, left, are defined by some preliminary work done by SRON [14] on the design of the copper support of the TES array. This structure has 5 potential locations for the wirebonds as highlighted in yellow in Fig. 4, left. Each location is numbered from *wb0* to *wb4* and tested in the thermal model. Figure 4, right, shows the temperature elevation at the center of the array for each of these designs independently. The impact of the CR hit is reduced by 30% for a wirebonding closer to the TES array compared to one on the edge of the frame. In the case of the *wb1* configuration, the wirebonds are placed 10 mm away from the array.

An important parameter in this model is the thermal conduction between the wafer and the ADR bath temperature. It can be increased by adding more Au wirebonds. However, the space is limited and the bonding process time needs to

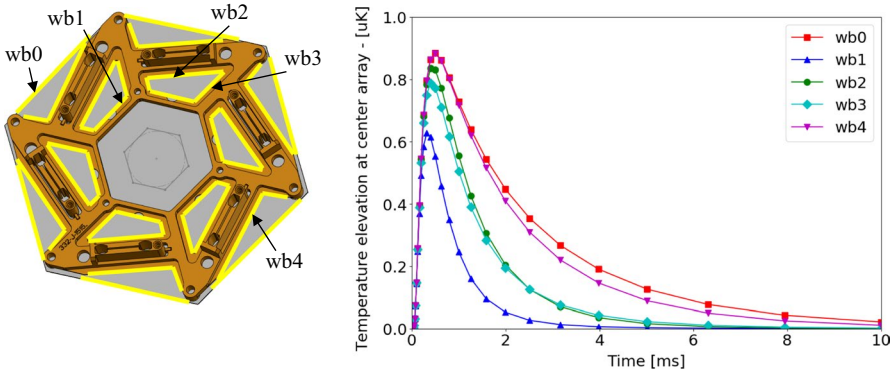

Fig. 4 Left, potential locations (highlighted in yellow) for wirebonds on the TES wafer support structure. This shows the back of the wafer. This preliminary design has been provided by Henk van Weers, SRON. Right, temperature elevation for the different wirebonding locations for a 150 keV cosmic ray impact at 18 mm away from the center (Color figure online)

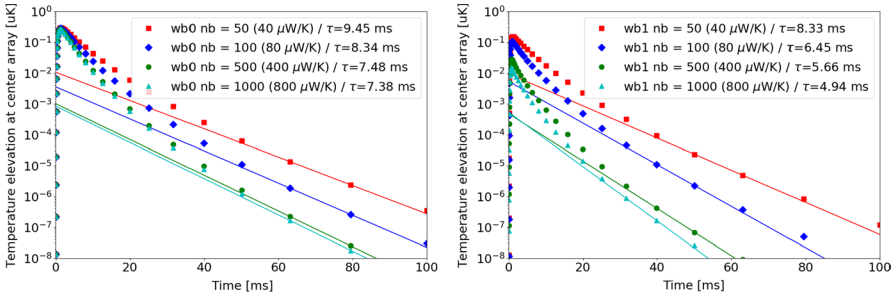

Fig. 5 Temperature elevation for 50, 100, 500 and 1000 wirebonds for the configuration *wb0*, with the wirebonds on the outer edge of the TES wafer (left) and the configuration *wb1*, with the wirebonds closer to the TES array, 10 mm away (right). Both cases are for a CR hit of 150 keV at 30 mm from the center of the TES array. The slower time constant τ of the temperature decay is given as well (Color figure online)

be taken into account. To determine the correct number of wirebonds, we run the thermal model for different amounts between 50 and 1000 wirebonds, giving a thermal conduction between 40 and 800 μW/K. Both configurations, with the wirebonds on the edge of the frame (*wb0*) or near the TES array (*wb1*), are simulated. The results, presented in Fig. 5, show that the temperature elevation amplitude decrease with higher number of wirebonds and the time constant τ decreases. Only the last time constant of the temperature decay is measured since it is dominated by the thermal link between the TES wafer and the ADR thermal bath. For the configuration *wb0*, we can notice that an amount of 500 wirebonds is sufficient to ensure a proper heat sinking, while this value goes to 1000 for the *wb1* configuration.

3.3 Additional Gold Coating and Position of the Wirebonds

The first geometry that we studied is based on an Au coating of 3.5 μm and 500 wirebonds at the position *wb0*, on the outer ring of the frame. The temperature increase at the center of the array for a 150 keV particle hitting 30 mm away is approximately 0.26 μK as shown in Fig. 6, right. With a required thermal sensitivity of 0.15 eV/μK and the high number of events of higher energies than 150 keV, we can expect a significant impact on the thermal stability of the bath.

To decrease the impact of the deposited energy by CRs, we have considered increasing the thickness of the backside Au plating to 6 μm and replacing the outer wirebonds (*wb0*) with some located closer to the TES array (*wb1*). For these two configurations, the temperature increase is 0.17 μK and 0.02 μK, respectively. The wirebonds at the *wb1* location, near the TES array, dominate the drain of the energy deposited by the CR. Thus, adding 2.5 μm of gold to this design decreases the amplitude of the temperature excursion by 10%, but make the chip fabrication more complex.

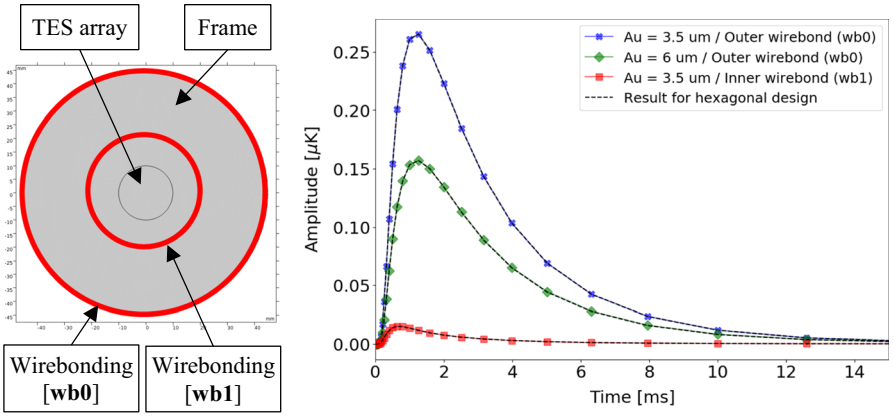

Fig. 6 Left, circular variant of the model in order to obtain a rotational symmetry. The CR hit is located at a distance d and an angle θ from the studied point at the center of the TES array. Two wirebonding designs are represented: on the outer edge of the wafer (*wb0*) and 10 mm away from the array (*wb1*). Right, Comparison of the thermal impact of a 150 keV particle hitting at $d=30$ mm and $\theta=0°$ for three different configurations with different thicknesses of Au coating (3.5 and 6 μm) and different wirebonding locations. The dashed line for each set of data corresponds to the simulated bath temperature for a hexagonal geometry instead of a disk geometry (Color figure online)

Placing the wirebonds closer to the TES array drains the heat flow from temperature pulse in the frame toward the heat sink, before it reaches the array. This configuration, composed of the inner wirebonding (*wb1*), 3.5 μm of Au plating and without the outer wirebonding (*wb0*) is considered as the *baseline* since it shows the lowest thermal impact at the center of the TES array.

3.4 Histogram Comparison

We computed the temperature excursion spectra for the whole range of deposited energies (see Fig. 1) at a random location in the frame by:

1. Simulate the temperature excursions with the FEM model for several points of distance d from the TES array center (11, 12, 13, 15, 19, 25, 30, 35, 40, 44 mm) and angle θ (0, 45, 90°). See Fig. 7, left.
2. Interpolate the temperature excursions at the center of the array using the results from the FEM model for all the events computed by the GEANT4 model

This algorithm is run 10 times through the GEANT4 events list for random hit location to increase statistics results.

To understand the thermal impact of the whole spectra of deposited energies each of the events extracted from the GEANT4 model is associated with a random distance d from 10 to 45 mm at a random angle θ, which covers the surface of the frame. The thermal increase at the center of the array is then interpolated for each hit location from the simulated energy deposition data of the thermal model. Since

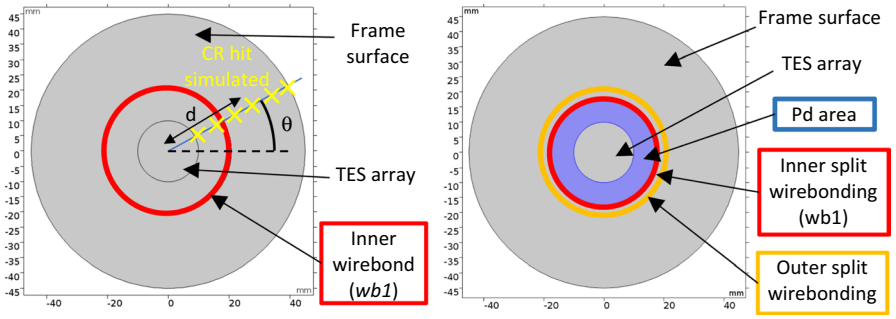

Fig. 7 Diagram of the two configurations studied. The frame is on the outer part of the wafer. The TES array is represented as a plain surface. Configuration with only the inner wirebonding (wb1) used as a reference (left). The second configuration (right) has a split coating of Au with an extra layer of Pd only outside of the TES array. The split requires a second wirebonding on the outer part of the wafer. On the left figure is given an example of locations of CR hits simulated in the FEM model, at different distances d and an angle θ (Color figure online)

the temperature excursion is linear with the energy, only the case for 500 keV deposited is simulated.

The distribution of temperature rises is plotted as a histogram (Fig. 8, left) for the *baseline* configuration which shows a rate of ~17.6 cps for events above 1 μK. This rate could impact the energy resolution of the detector [13], assuming a thermal stability of 0.15 eV/μK. To further reduce the impact of the CRs and to keep the predicted energy resolution within the error budget allocation, two further design iterations may be required: (1) increasing the heat capacity of the substrate thermal bath through an additional layer of Pd (on top of the Au layer) on the coating outside of the TES array which has a specific heat capacity 17 times higher than that of gold, (2) splitting the Au coating outside of the region of the TES array to reduce the heat flowing from the frame to the TES array. The two cases are represented in Fig. 7. Our modeling suggests that implementing these two features could allow us to decrease the number of events above 1 μK by more than a factor 10 to ~1.5 cps. The amplitude of the temperature increase as a function of the distance shows the effect of the split in the coating (Fig. 8, right).

The impact of the change of bath temperature of the TES on the energy resolution of a 7 keV line for these two designs is available in the accompanying contribution to these proceedings [13].

4 Study of CR Impact on the Muntins

Even though the model is primarily designed to study the interaction of CR with the Si frame (outside of the TES array), we also studied the thermal impact of the CR interacting near the TES sensor within the array. A more realistic 2D design of the muntins has been added to the model with a high-density mesh. To represent most of the cases, an energy pulse of 150 keV, representing the peak of the spectrum

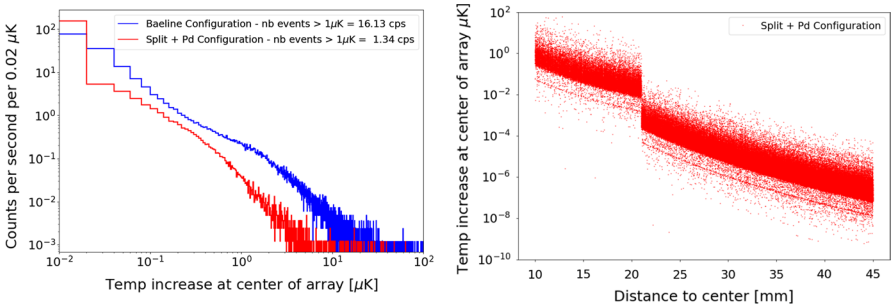

Fig. 8 Left, histogram of temperature increase in the Si at the center of the wafer. The baseline configuration (blue) is for a 3.5 μm thickness of Au coating and 1000 wirebonds positioned near the TES array (*wb1*). The second configuration (red) has a split coating composed of two layers of 4 μm Pd and 2 μm Au. The split is outside of the TES array, 22 mm away from the center. Right, temperature increase at the center in function of the distance of the hit of the CR for the featured configuration. The impact of the split of the coating is obvious here with a decrease in an order of magnitude between inside and outside of the split (Color figure online)

(Fig. 1), is deposited at the intersection of 4 muntins at the center of the array. The results presented in Fig. 9 show the modeled temporal profile of the bath temperature for various distances between a particular muntin position (such as that of a microcalorimeter) and the CR event, considering distances between 0 mm to 2 mm away. One can see that the temperature can rise up to a significant fraction of 1 K. However, the time constant of the event is very short. After ~30 μs all temperature profiles coincide and after 1 ms, the temperature excursions everywhere in the array are below 1 μK.

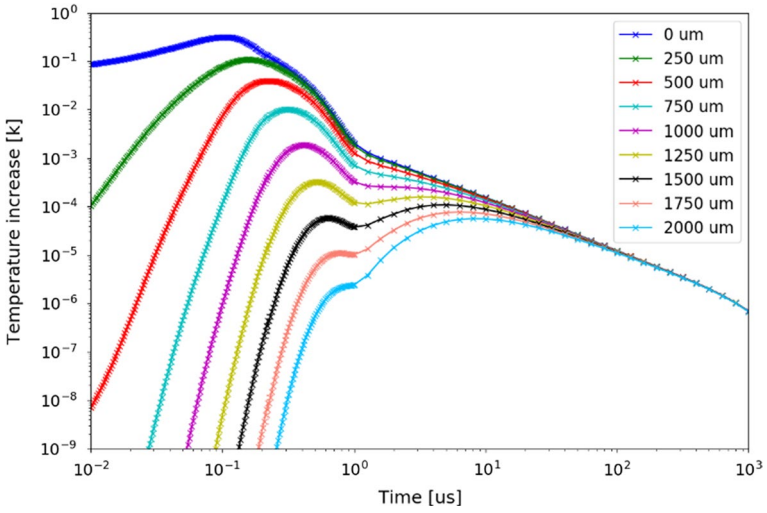

Fig. 9 Temperature profiles for a CR hit at the center (0 μm) at each muntin intersection up to 2 mm (Color figure online)

According to the GEANT4 model, these events will occur 6 times per second with a range of energy depositions. Relatively low energy events may create thermal crosstalk with nearby pixels [15] while large ones can and will need to be flagged and removed from the data [13].

5 Conclusion

The configuration with the wirebonds incorporated close to the TES array (wb1) produces a significant decrease in the temperature rise seen at the center of the TES array compared with wirebonds located on the edge of the wafer. The number of bonds needed to provide the best thermal link between the chip and the ADR thermal bath is in the order of 1000 in order to provide a total thermal conductance to the heat bath of 800 μW/K. With this configuration and based on the deposited energy spectra generated by the GEANT4 simulations, the rate of events above 1 μK is about 17 cps. To reduce this value, we implemented an additional layer of Pd to the back surface of the substrate in addition to the planned Au and a split in the coating. Our models show a decrease in the rate of events above 1 μK by a factor 10, down to 1.5 cps. Incorporating these features will decrease the impact of CR to meet the energy-resolution budget of 0.2 eV for this mechanism, thereby improving the energy resolution of the microcalorimeter pixels.

Interpolation tables for both configurations have been provided to the X-IFU End-to-End simulator team. The impact of the change of bath temperature of the TES on the energy resolution of a 7 keV line for these two designs has been simulated. The effect on the energy reconstruction is 0.06 eV for the configuration with inner wirebonds (wb1) and 0.03 eV for the configuration with both the additional Pd and the coating split. Further details are available in the accompanying contribution to this proceeding [13].

References

1. K. Nandra et al., (2013). arXiv:1306.2307 [astro-ph.HE]
2. D. Barret et al., in *Proceedings SPIE, Space Telescopes and Instrumentation 2014: Ultraviolet to Gamma Ray*, vol. 9905 (2016), p. 99052F. https://doi.org/10.1117/12.2232432
3. E.E. Vos, M.S. Potgieter, Sol. Phys. **291**, 2181 (2016). https://doi.org/10.1007/s11207-016-0945-7
4. S. Lotti et al., in *Proceedings SPIE, Space Telescopes and Instrumentation 2016: Ultraviolet to Gamma Ray*, vol. 9905 (2016), p. 990563. https://doi.org/10.1117/12.2232381
5. S. Lotti et al., in *Proceedings SPIE, Space Telescopes and Instrumentation 2018: Ultraviolet to Gamma Ray*, vol. 10699 (2018), p. 106991Q. https://doi.org/10.1117/12.2313236
6. S. J. Smith et al., in *Proceedings SPIE, Space Telescopes and Instrumentation 2016: Ultraviolet to Gamma Ray*, vol. 9905 (2016), p. 99052H. https://doi.org/10.1117/12.2231749
7. C. Macculi et al., in *Proceedings SPIE, Space Telescopes and Instrumentation 2016: Ultraviolet to Gamma Ray*, vol. 9905 (2016), p. 99052K. https://doi.org/10.1117/12.2231298
8. COMSOL Multiphysics, v. 5.4, COMSOL AB, Stockholm, Sweden. www.comsol.com. Accessed 2019
9. C. Kilbourne et al., J. Astron. Telesc. Instrum. Syst. **4**(1), 011214 (2018). https://doi.org/10.1117/1.JATIS.4.1.011214

10. J. Wilms et al., in *Proceedings SPIE, Space Telescopes and Instrumentation 2014: Ultraviolet to Gamma Ray*, vol. 9144 (2014), p. 91445X. https://doi.org/10.1117/12.2056347
11. P. Peille et al., in *Proceedings SPIE, Space Telescopes and Instrumentation 2016: Ultraviolet to Gamma Ray*, vol. 9905 (2016), p. 99055W. https://doi.org/10.1117/12.2232011
12. J. Wilms et al., in *Proceedings SPIE, Space Telescopes and Instrumentation 2016: Ultraviolet to Gamma Ray*, vol. 9905 (2016), p. 990564. https://doi.org/10.1117/12.2234435
13. P. Peille et al., J. Low Temp. Phys. (2020). https://doi.org/10.1007/s10909-019-02330-3
14. B.D. Jackson et al., in *Proceedings SPIE, Space Telescopes and Instrumentation 2016: Ultraviolet to Gamma Ray*, vol. 9905 (2016), p. 99052I. https://doi.org/10.1117/12.2232544
15. A. Miniussi et al., J. Low Temp. Phys. (2020). https://doi.org/10.1007/s10909-019-02312-5